International Journal of Biological Macromolecules 163 (2020) 776–787

Contents lists available at ScienceDirect

International Journal of Biological Macromolecules

journal homepage: http://www.elsevier.com/locate/ijbiomac

Structural analysis of a glucoglucuronan derived from laminarin and the mechanisms of its anti-lung cancer activity

Weihua Jin [a,b], Xinyue He [a], Wanli Wu [a], Yizhong Bao [c], Sanying Wang [c], Min Cai [a], Wenjing Zhang [d], Chunyu Wang [b,e], Fuming Zhang [b], Robert J. Linhardt [b,e], Genxiang Mao [c,*], Weihong Zhong [a,*]

[a] College of Biotechnology and Bioengineering, Zhejiang University of Technology, Hangzhou 310014, China
[b] Department of Chemical and Biological Engineering, Center for Biotechnology and Interdisciplinary Studies, Rensselaer Polytechnic Institute, Troy, NY 12180, USA
[c] Zhejiang Provincial Key Lab of Geriatrics, Department of Geriatrics, Zhejiang Hospital, Hangzhou 310013, China
[d] Department of Endocrinology, Sir Run Run Shaw Hospital, Zhejiang University School of Medicine, Hangzhou 310016, China
[e] Department of Biological Science, Departments of Chemistry and Chemical Biology and Biomedical Engineering, Center for Biotechnology and Interdisciplinary Studies, Rensselaer Polytechnic Institute, Troy, NY 12180, USA

ARTICLE INFO

Article history:
Received 23 May 2020
Received in revised form 5 July 2020
Accepted 7 July 2020
Available online 10 July 2020

Keywords:
Glucoglucuronan
Laminarin
Anti-lung cancer activity

ABSTRACT

Laminarin (LA), a storage glucan, was purified from the brown alga *Sargassum thunbergii*. After specific oxidation using the stable nitroxyl radical, 2,2,6,6-tetramethylpiperidine-1-oxyl (TEMPO), together with NaBr and NaClO, glucoglucuronan (LAO) was obtained. Compositional analysis of LAO showed a molar ratio of glucuronic acid (GlcA) to glucose (Glc) of 12.7: 1. Nuclear magnetic resonance (NMR) and mass spectroscopy (MS) showed LAO to have a backbone of (1 → 3)-linked β-D-Glc*p*A interspersed with (1 → 3, 1 → 6)-linked β-D-Glc*p*, that was terminated with β-D-Glc*p*A. LAO inhibited human lung cancer A549 cell proliferation *in vitro*. IC_{50} values at 12 h and 24 h were 2.70 mg/mL and 2.85 mg/mL, respectively. Western blotting showed that TSC2 was up-regulated at an LAO concentration of 3.80 mg/mL. FAK, PI3K, P-AKT and mTOR were down-regulated, indicating LAO inhibited cancer cell proliferation through the FAK/PI3K/AKT/mTOR pathway. Surface plasmon resonance (SPR) studies revealed that LAO showed an IC_{50} of 0.07 mg/mL inhibiting the binding of heparin to fibroblast growth factor 1 (FGF1) LAO inhibition of heparin binding to FGF2 fluctuated between 15% and 28%, suggesting that LAO inhibits A549 cell proliferation by selectively interacting with FGF1.

1. Introduction

Laminarin, also called alminaran, is a storage glucan required for the maturation in brown algae [1]. The amount of laminarin changes over the life cycle of algae. Many studies [2–10] suggest laminarin for biomedical application such as anti-cancer activity, immune stimulatory effects, anti-angiogenesis activity, in tissue engineering applications, anti-oxidant and anti-inflammatory activities. Laminarin can be modified by irradiation, sulfation, acylation and reduction [2]. Sulfated laminarin has been used as radioprotectors and radiosensitizers in melanoma therapy [11], and has also exhibited anti-complement activity [12]. Hydrophobized laminarin, prepared through polysaccharide acylation, represents a biocompatible anti-oomycete compound for grapevine protection [13]. Laminarin decorated selenium nanoparticles showed cytotoxicity towards HepG2 cells through autophagy and by inducing apoptosis [14]. Methacrylated laminarin microparticles provide an effective support for cell attachment and expansion [15].

TEMPO-mediated reaction has been widely used for the oxidation of oat β-D-glucan [16], lignin [17], softwood cellulose [18–20], curdlan [21], cornstarch [22], and chitin [23]. TEMPO-mediated reactions are useful for determining the degree of substitution at the C6 position in different modified polysaccharides because it selectively oxidizes primary hydroxyl groups [21,24]. Many protected saccharide derivatives have also been converted, using TEMPO-mediated oxidation, into uronic acid derivatives as GAG mimetics [19]. There are no studies on the oxidation of laminarin from brown algae.

There are a number of reports on glucoglucuronans. Guentas et al. [25] used *Rhizobium sp.* T1 strain to produce a glucoglucuronan, which has a → 3)-β-D-Glc*p*A-(1 → 4)-β-D-Glc*p*-(1 → disaccharide backbone. The position of the sulfate groups in this glucoglucuronan (primary or secondary hydroxyl group) had no influence on its regenerating activity on injured rat *extensor digitorum longus* (EDL) muscles, but acetylation of this glucoglucuronan modulates EDL activity [26]. Moreover, TEMPO-mediated oxidation and sulfation of this glucoglucuronan affords glycosaminoglycan mimetics [27].

Laminarin is a (1 → 3, 1 → 6)-linked β-D-glucan [28]. In the current study we describe the preparation of a new glucoglucuronan (LAO) using a TEMPO-mediated reaction. Structural analysis of LAO relied on

* Corresponding authors.
E-mail addresses: maogengxiang@163.com (G. Mao), whzhong@zjut.edu.cn (W. Zhong).

https://doi.org/10.1016/j.ijbiomac.2020.07.069
0141-8130/

high performance liquid chromatography (HPLC), mass spectrometry (MS) and one-dimensional (1D) and two-dimensional (2D) nuclear magnetic resonance (NMR) spectroscopy. The anticancer activity of LAO was tested *in vitro* for inhibiting the proliferation of A549 cells by impacting protein expression in the FAK/PI3K/AKT/mTOR pathway to elucidate the mechanism anti-lung cancer activity of LAO. SPR was used to analyze LAO inhibition of fibroblast growth factor (FGF1 and FGF2) binding to heparin. We elucidate the structure of LAO and demonstrate the mechanism of its anti-lung cancer activity, suggesting its utility in anticancer drug development.

2. Materials and methods

2.1. Materials

The brown algae *Sargassum thunbergii* was collected in Dongtou, China. The L-fucose (Fuc), D-galactose (Gal), D-mannose (Man), D-glucuronic acid (GlcA), L-rhamnose monohydrate (Rha), D-xylose (Xyl), D-glucosamine (GlcN), D-*N*-acetylglucosamine (GlcNAc), D-galactouronic acid (GalA) and D-glucose (Glc) standards and 3-methyl-1-phenyl-2-pyrazolin-5-one (PMP) (99%) were purchased from Sigma Aldrich (St. Louis, MO). Recombinant human FGF1 and FGF2 were gifts from Amgen (Thousand Oaks, CA).

2.2. Preparation and purification of laminarin (LA)

Crude polysaccharide (ST) was prepared according to a previous study [29]. ST was fractionated by anion exchange chromatography on a DEAE-Bio Gel Agarose FF gel (6 cm × 40 cm), eluted with water (5 L) dialyzed, concentrated, and precipitated to obtain crude laminarin. Crude laminarin was purified by repeating the above procedure a second time to obtain purified LA.

2.3. Preparation of oxidized laminarin (LAO)

Oxidized laminarin (LAO) was prepared from purified LA based on the modification of a previous method [30]. Briefly, 1 g of purified LA dissolved in 50 mL water was heated at 80 °C, then cooled to 25 °C and TEMPO (32 mg) and NaBr (320 mg) were added. The reaction was adjusted to pH 10 and a NaClO (12 mL, XM) solution was added over 4 h after which ethanol was added to terminate the reaction. The mixture was dialyzed by 500 Da molecular weight cut-off (MWCO) dialysis bag at pH 5, concentration, and lyophilization. The product obtained (1 g) was degraded with 1 M trifluoroacetic acid (10 mL) for 1 h at 100 °C, dialyzed, concentrated, and lyophilized to obtain LAO.

2.4. Composition, MS and NMR analysis

The molar ratio of monosaccharides was determined based on a previous study [31]. The molecular weights of the polysaccharides were evaluated by gel permeation chromatography (GPC)-high performance chromatography (HPLC) on TSK G3000 PWxl column (7 μm, 7.8 × 300 mm) with elution in 0.05 M Na_2SO_4 at a flow rate of 0.5 mL/min at 40 °C and detected by refractive index. Ten different molecular weight dextran standards were purchased from the National Institute for the Control of Pharmaceutical and Biological Products (Beijing, China).

Electrospray ionization (ESI)-mass spectrometry (MS) and ESI-collision induced dissociation (CID)-MS^n were performed on a LTQ ORBITRAP XL (Thermo Scientific, Waltham, MA, USA). The samples were dissolved in CH_3CN-H_2O (1,1, *v*/v). The solution was centrifuged, and the supernatant was analyzed. Mass spectra were obtained in the negative-ion mode at a flow rate of 5 μL/min. The capillary voltage was set to −3000 V, and the cone voltage was set at −50 V. The source temperature was 80 °C, and the desolvation temperature was 150 °C. The collision energy was optimized between 10 and 50 eV. All spectra were analyzed by Xcalibur.

Polysaccharides (50 mg) were co-evaporated with deuterium oxide (99.9%) twice before dissolving in deuterium oxide (99.9%) containing deuterated acetone. One and two dimensional spectra, including ^{1}H NMR, distortionless enhancement by polarization transfer including the detection of quarternary nuclei (DEPTQ), ^{1}H-^{1}H correlated spectroscopy (COSY), ^{1}H-^{13}C heteronuclear single quantum coherence spectroscopy (HSQC), ^{1}H-^{13}C heteronuclear multiple bond correlation spectroscopy (HMBC) and ^{1}H-^{1}H total correlation spectroscopy (TOCSY), were recorded at a Bruker AVANCE III 600 MHz at 25 °C. The chemical shifts were adjusted to the internal standard (deuterated acetone, 2.05 and 29.92 ppm, respectively). The NMR experiment parameters are as follows: ^{1}H NMR: spectral width (8012.8 Hz), relaxation delay (1 s), acquisition time (2.045 s), scans (32); DEPTQ: spectral width (31,250.0 Hz), pulse tip angle (45 degrees), C13 relaxation delay (2 s), acquisition time (1.049 s), scans (2000); HSQC: spectral width (F2: 8012.8 Hz; F1: 25133.5 Hz), relaxation delay (1 s), acquisition time (0.150 s), complex points (1202); ^{1}H, ^{1}H-COSY: spectral width (F2: 2907.0 Hz), relaxation delay (1 s), acquisition time (0.150 s), complex points (436); HMBC spectral width (F2: 8012.8 Hz; F1: 30165.9 Hz), relaxation delay (1 s), acquisition time (0.150 s), complex points (1202) and TOCSY: spectral width (F2: 2907.0 Hz), relaxation delay (1 s), acquisition time (0.150 s), complex points (436).

2.5. The proliferation inhibition activity and transwell migration assay

The proliferation inhibition activities of LAO against human lung cancer A549 cells were determined. A 3-(4, 5-dimethylthiazol-2-yl)-2, 5-diphenyl tetrazolium (MTT) assay was used to measure cell viability. The cells were divided into two groups: (1) a control group in which cells were cultivated in blank medium; and (2) an experimental group LAO was added at different concentrations and cells were cultivated in medium. Inhibition was determined using the following equation: Cell Inhibition (%) = (Ac − A1)/(Ac − A0) × 100, where A0 was the absorbance of the blank medium (no cells), A1 was the absorbance in the presence of samples, and Ac was the absorbance of the control.

Transwell migration assay was performed based on a previous study [32]. A549 cells were transferred into the upper compartment. The chamber was washed with PBS after 24 h incubation and fixed with 4% paraformaldehyde. Then, the chamber was washed again and stained by 4′, 6-diamidino-2-phenylindole (DAPI). Finally, the chamber was washed and photographed with ZEISS Axio Zeiss Vert. A1 microscope (Jena, Germany), counted in five random fields. The migrating cells (% of the control) were calculated as follows: N/N0 × 100, where N0 was the number of cells in the control group, N was the number of cells in the experiment group.

2.6. Western blot analysis

Immunoblotting analysis was carried out based on a previously described protocol [33]. The cells were washed with ice old PBS and lysed with lysis buffer containing protease inhibitors cocktail from Cell Signaling Technology, Inc. (Danvers, MA, USA). Protein concentrations were determined by BCA assay. Proteins were loaded and subjected to electrophoresis on an SDS polyacrylamide gel and transferred to a polyvinylidene fluoride (PVDF) membrane (Bio-Rad). The membranes were subsequently probed with anti-FAK, anti-Phospho-PI3 kinase, anti-AKT (pan), anti-phosphorylated Akt (Ser473) anti-Tuberin/TSC2, anti-mTOR and anti-β-Actin (Cell Signaling Technology, Inc., USA). Secondary antibody, used for detection, was linked with horseradish peroxidase. The enhanced chemiluminescence method was used to detect the conjugated horseradish peroxidase. The optical density for each ladder was obtained by Image J software and the relative change was calculated.

2.7. Solution competition study between heparin on chip surface and LAO in solution using surface plasmon resonance (SPR)

Solution competition SPR measurements were performed on a BIAcore 3000 (GE Healthcare, Uppsala, Sweden). A heparin chip was prepared according to the previous studies [34] by immobilization of biotinylated heparin on a streptavidin (SA) chip. FGF1 or FGF2 was premixed with different concentrations of LAO and injected over the heparin chip at 30 μL/min to measure the inhibition of LAO on fibroblast growth factors (FGF1 and FGF2) binding to heparin surface. In each run, after the dissociation period the chip was regenerated with 2 M NaCl.

2.8. Statistical analysis

All data are shown as the mean ± standard deviation (SD). Significant differences between experimental groups were determined by one-way ANOVA, and differences were considered as statistically significant if $p < 0.05$. All calculations were performed using SPSS 16.0 Statistical Software.

3. Results

3.1. Chemical composition and structure analysis

Laminarin (LA) was isolated from *Sargassum thunbergii*. The molecular weight of LA was about 4.8 kDa (Fig. 1A). The analysis of the molar ratio of monosaccharides (Fig. 1B) showed that LA consisted solely of Glc, indicating that it was a glucan. In the ^{1}H NMR spectrum (Fig. 2A), the chemical shifts at 4.6 and 4.4 ppm were assigned to the anomeric proton of the (1 → 3)-linked β-D-Glc*p* and (1 → 6)-linked β-D-Glc*p*, respectively. In the DEPTQ spectrum (Fig. 2B), resonances with chemical shifts at 103.0 (C-1), 73.9 (C-2), 84.7 (C-3), 68.6 (C-4), 76.1 (C-5) and 61.2 (C-6) ppm are characteristic of (1 → 3)-linked β-D-glucan. The weaker resonance with chemical shift at 70.1 (C-6) ppm corresponded to (1 → 6)-linked β-D-Glc*p*. In the HSQC spectrum (Fig. 2C), the position of the correlation peak H-1/C-1 at 4.5/96.1 ppm proved that the reducing end is a β-D-Glc*p*, not mannitol, which was confirmed by the absence of a chemical shift at 63.7 ppm [2,28,35,36]. The correlation peaks H1/C1 at 4.6/103.0 and 4.4/103.3 ppm were assigned to the anomeric protons/carbons of (1 → 3)-linked β-D-Glc*p* and (1 → 6)-linked β-D-Glc*p*, respectively. Therefore, we concluded that LA had a backbone of (1 → 3)-linked β-D-glucan, branched with (1 → 6)-linked β-D-Glc*p* and terminated with β-D-Glc*p*. After oxidation, the resulting LAO had a molecular weight (Fig. 1A) of approximately 5.7 kDa, higher than LA from which it was derived. The analysis of the molar ratio of monosaccharides (Fig. 1B) showed that LAO contained GlcA and Glc in a molar ratio of 12.7: 1. This ratio can be explained by LA having branches of Glc*p* at C6 that could not be oxidized. It has been reported [30] that primary hydroxyl groups of Glc*p* at position 6 are selectively oxidized to afford glucuronic acid residues in TEMPO-NaBr-NaClO mediated oxidation.

Detailed structure of LAO was determined by one and two-dimensional NMR spectroscopy in Figs. 2 and S1. The HSQC spectrum of LAO (Fig. 2D), showed one new correlation peak H-1/C-1 at 4.6/94.9 ppm. In the TEMPO-NaBr-NaClO mediated oxidation system, the primary hydroxyl groups (C6) of Glc*p* are selectively oxidized to be GlcA. However, the reducing end sugar ring of LA was also oxidized to a carboxyl group at the position 1 and the ring was opened (Scheme 1) [30]. According to previous study [21], the chemical shifts of the anomeric carbons of curdlan (curdlan is a linear glucan composed of (1 → 3)-linked β-D-Glc*p*) and oxidized curdlan were relatively stable. This new peak was assigned to the GlcA residues (Residue D) at the reducing end. The other two correlation peaks of LA and LAO in Fig. 2C and D at approximately 4.6/103 and 4.3/103 ppm were similar. Therefore, we suggest that the correlation peak at approximately 4.3/103 ppm was assignable to the anomeric proton/carbon of the (1 → 6)-linked β-D-Glc*p*A (Residue A) and the correlation peak at 4.6/103 ppm was assignable to the anomeric proton/carbon of the (1 → 3)-linked β-D-Glc*p*A (Residue B) and (1 → 3, 6)-linked β-D-Glc*p*A (Residue C). The presence of the correlation peak at 3.8,3.6/69.1 ppm corresponded to the H6/C6 of the Residue C. In conclusion, the assignments of the chemical shifts in LAO were summarized in Table 1. The degree of branching was 8%, which was calculated using the following equation: Degree of branching (%) = $1/(N-1) \times 100$, where N was the molar ratio of GlcA to Glc.

Next, the LAO was analyzed by MS. Fig. S2 shows the negative-ion mode ESI-MS spectrum of LAO. From previous studies [30,37], it was concluded that the primary hydroxyl groups at position 6 are selectively oxidized to afford GlcA residues in the TEMPO-NaBr-NaClO mediated oxidation reaction, and this was also accompanied with a ring-opened reducing terminal sugar as summarized in Scheme 1. Table 2 shows the MS of LAO contains glucuronan and its derivatives. ESI-CID-MS^n was further performed to elucidate the glucuronan structures.

The fragmentation patterns included fragment ions at *m/z* 513.074 (−2), 601.091 (−2) and 689.104 (−2) that were similar to the ion at *m/z* 425.58 (−2). The identification of the fragmentation of the ion at *m/z* 425.058 (−2) as $[GlcA_4OX_3–2H]^{2-}$is shown in Fig. 3A. The intense fragment-ion at *m/z* 394.057 (−2) included the loss of CO_2 and H_2O. There are several characteristic ions at 175.025 (B_1), 369.067 (C_2), 545.099 (C_3), 675.089 (Y_3) and 703.120 (B_4). In addition, there was no characteristic ^{0,2}A ion, indicating a 1 → 3 linkage, which is consistent with NMR results. The fragment ions at *m/z* 338.048 (−2) and 403.062 (−2) included the loss of CO_2 and a C-type ion and molecular ion, indicating a decarboxylation process. Moreover, ESI-CID-MS^3 was performed to elucidate the structure of the intensive fragment ion at *m/z* 394.057 in Fig. 3B. Four types of fragment ions were observed, B-type, C-type, Y-type and Z-type ions. The fragment ions at *m/z* 325.041 and 501.073 derived from the loss of CO_2 from a C-type ion. Thus, we concluded that the molecular ion at *m/z* 425.058 (−2) corresponded to GlcA (1 → 3) GlcA(1 → 3) GlcA(1 → 3) GlcA(1 → 3)OX_3.

The fragmentation pattern of the fragment ions at *m/z* 395.055 (−2), 535.087 (−2), 623.103 (−2) and 711.120 (−2) were similar to the ion at *m/z* 447.071 (−2). The fragmentation of the ion at *m/z* 447.071 (−2), $[GlcA_4OX–2H]^{2-}$is shown in Fig. 3C. Three ion types, B-type, C-type and Y type were observed. In addition, some ions derived from the loss of CO_2 were also observed. It was also similar to the fragmentation pattern of the fragment ion at *m/z* 425.058 (−2). Further studies on the fragment ions at *m/z* 416.070 $[GlcA_4OX\text{-}CO_2\text{-}H_2O\text{-}2H]^{2-}$ (Fig. 3D) and 719.115 $[GlcA_4OX\text{-}GlcA\text{-}H]^{1-}$ (Fig. 3E) were performed by ESI-CID-MS^3. Both showed the same type ions. Therefore, we conclude that the molecular ion at *m/z* 447.071 (−2) is GlcA(1 → 3) GlcA(1 → 3) GlcA (1 → 3) GlcA(1 → 3)OX.

LA has a backbone of (1 → 3)-linked β-D-glucan, branched with (1 → 6)-linked β-D-Glc*p* and terminated with β-D- Glc*p*. And TEMPO-NaBr-NaClO mediated oxidation system could selectively oxidized C6 of Glc*p*. Thus, we propose a reaction of LAO shown in Scheme 1.

3.2. Anti-tumor activity of LAO

A549 cells were exposed to increasing concentrations of LAO for 12 and 24 h, and cell viability was measured by MTT assay to evaluate the proliferation inhibition by LAO. LAO markedly inhibited the growth of A549 cells in a dose-dependent manner (Fig. 4A). The IC_{50} values at 12 h and 24 h were calculated to be 2.70 mg/mL and 2.85 mg/mL, respectively. In addition, transwell migration assay was performed. The results (Fig. 4B and C) revealed that LAO could significantly inhibit the migration at the concentration of 1.5 mg/mL.

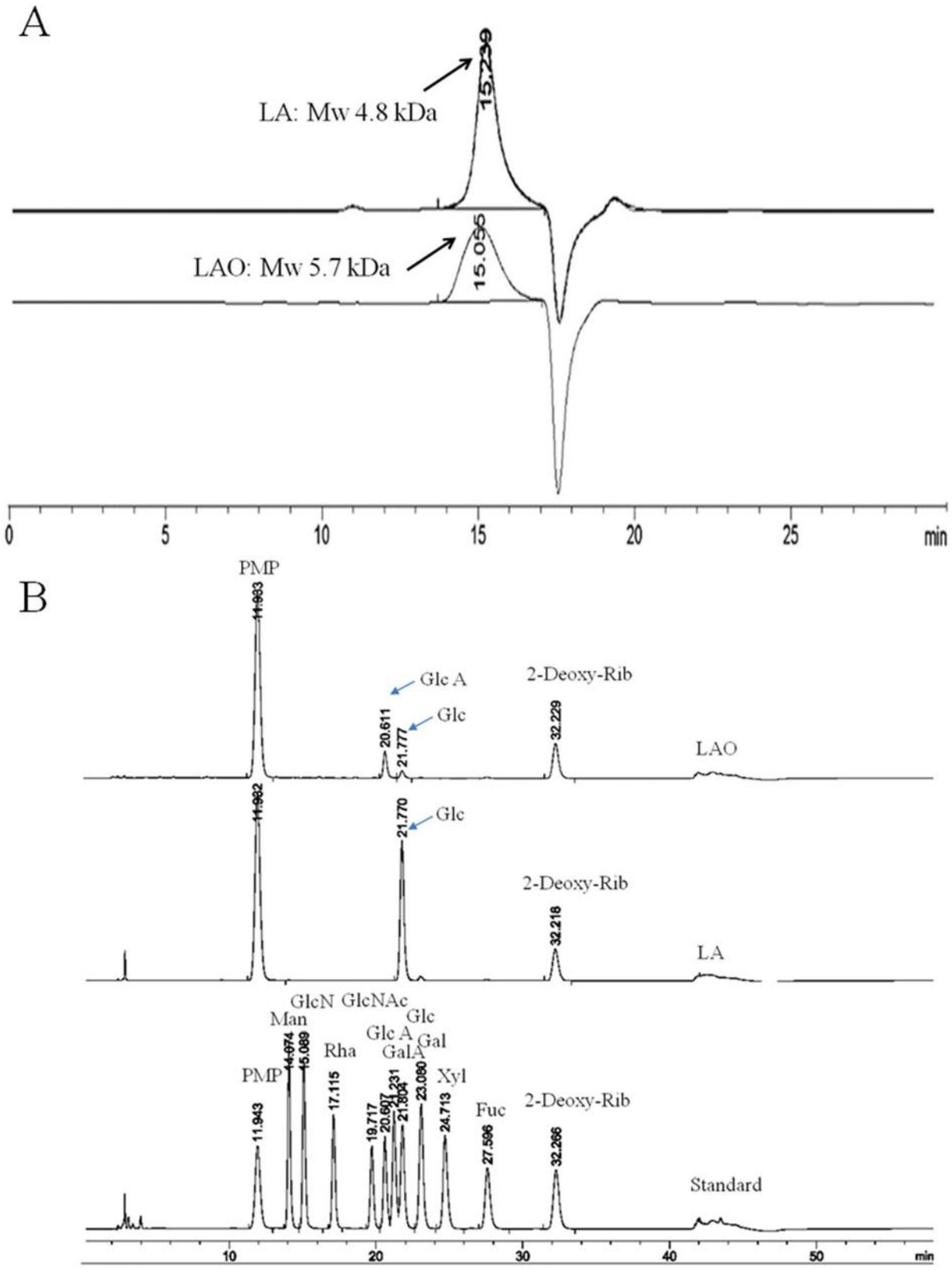

Fig. 1. The gel performance chromatography (GPC)-HPLC chromatograms of LA and LAO (A) and HPLC chromatograms of 1-phenyl-3-methyl-5-pyrazolone (PMP) derivatives of monosaccharides of LA and LAO (B). The sequences of the peaks are as follows: PMP, mannose (Man), glucosamine (GlcN), rhamnose (Rha), *N*-acetylglucosamine (GlcNAc), glucuronic acid (GlcA), galactouronic acid (GalA), glucose (Glc), galactose (Gal), xylose (Xyl), fucose (Fuc), 2-deoxy-D-Ribose (2-Deoxy-Rib).

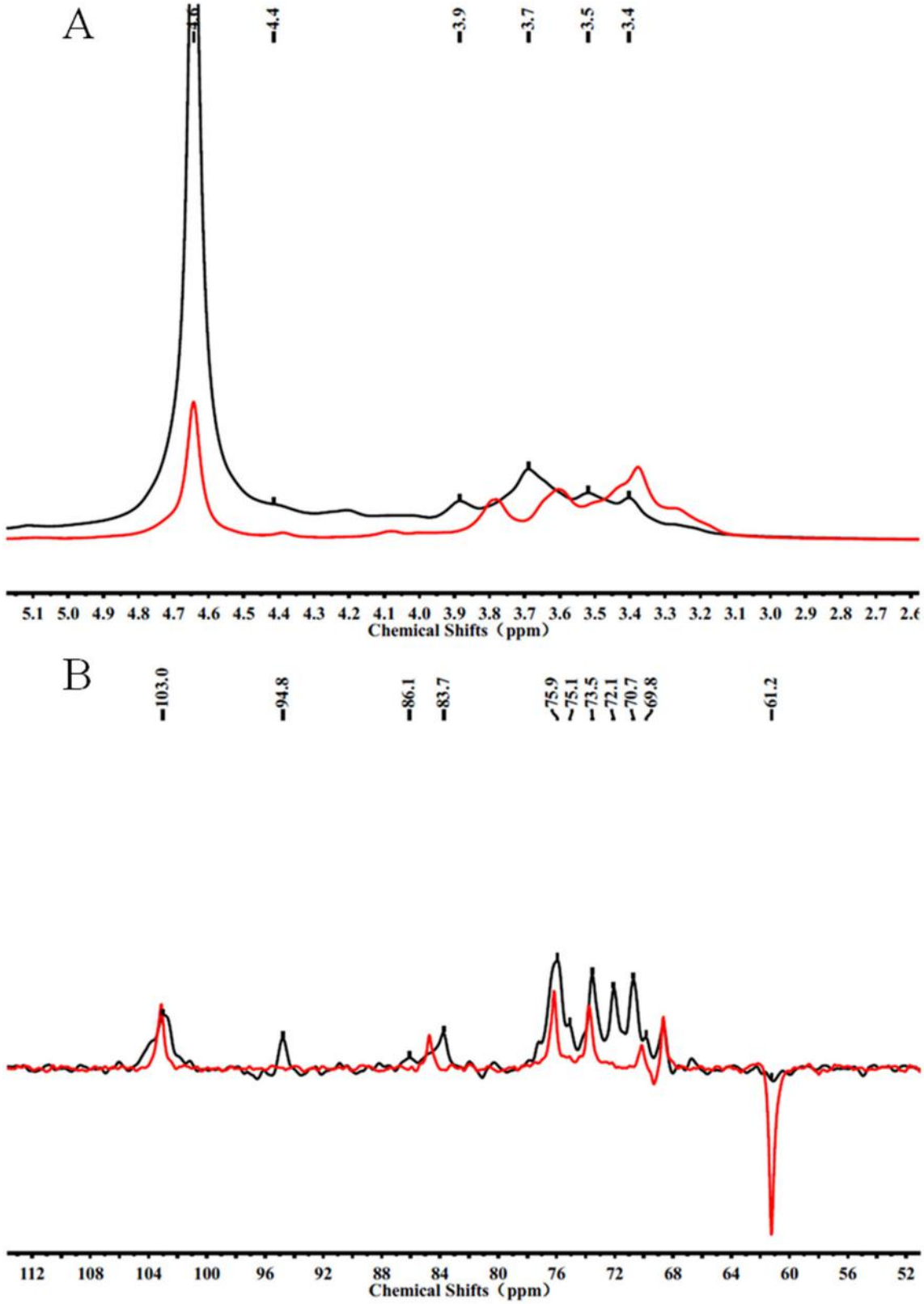

Fig. 2. The ^{1}H NMR (A: Red for LA, Black for LAO), DEPTQ (B: Red for LA, Black for LAO) and HSQC (LA: C and LAO: D) spectra. (For interpretation of the references to colour in this figure legend, the reader is referred to the web version of this article.)

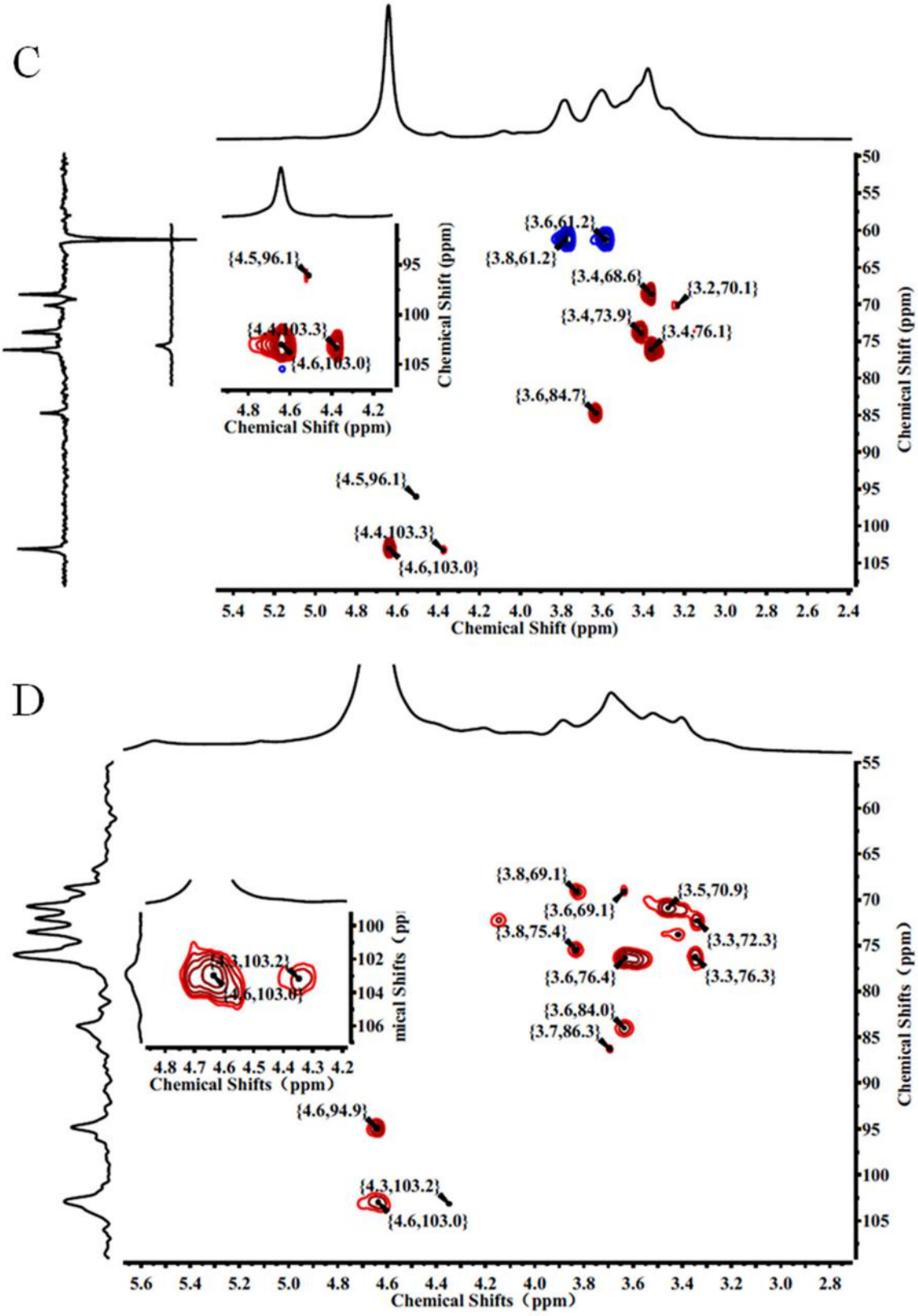

Fig. 2 (*continued*).

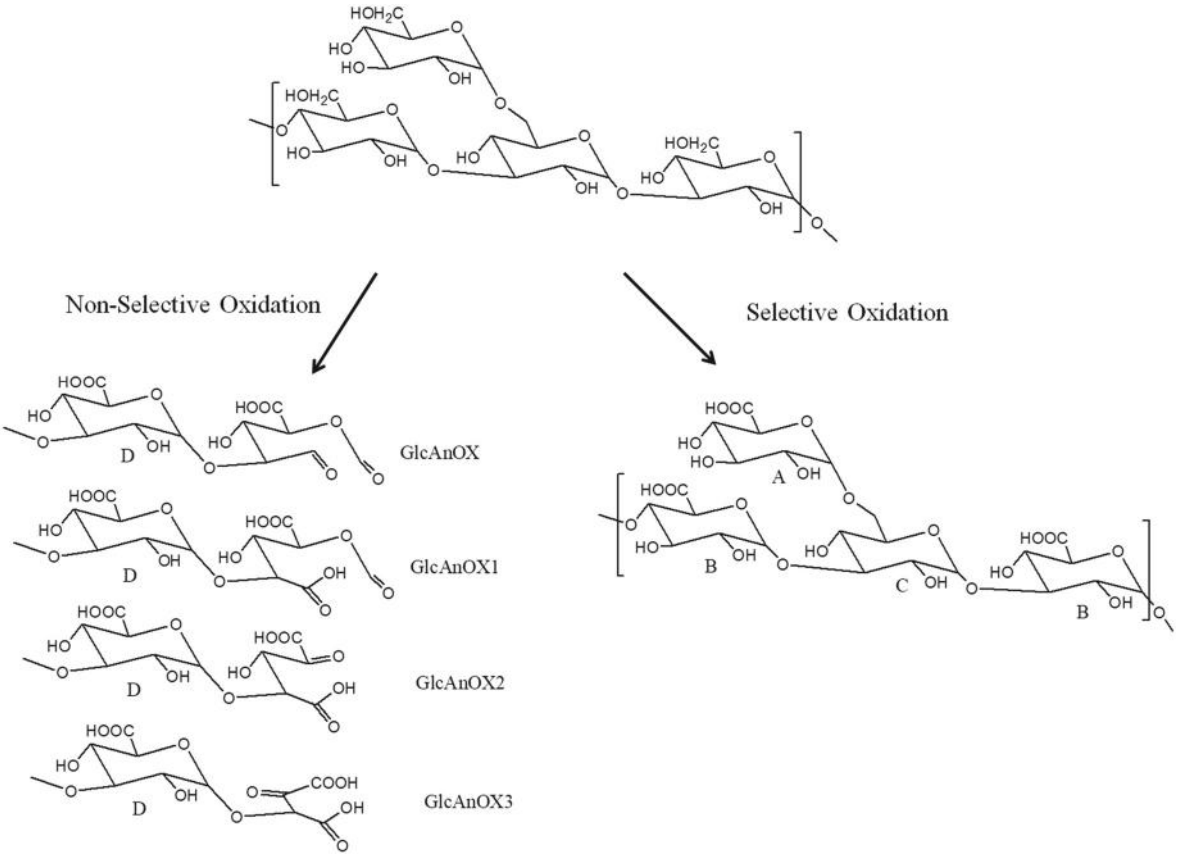

Scheme 1. Summary of LA and LAO in the course of oxidation

Table 1
^{1}H and DEPTQ chemical shifts for LAO.

Residues	H1/C1	H2/C2	H3/C3	H4/C4	H5/C5	H6/C6
A: β-D-Glc*p*A-(1 → 6	4.3/103.2	3.40/73.8	3.40/75.9	3.5/70.9	3.6/76.4	−/175.6
B: →3)- β-D-Glc*p*A-(1 → 3	4.6/103.0	3.3/72.3	3.6/84.0	3.5/70.9	3.6/76.4	−/175.6
C: →3,6)- β-D-Glc*p*-(1 → 3	4.6/103.0	3.3/72.3	3.7/86.3	3.5/70.9	3.8/75.4	3.8,3.6/69.1
D: →3)- β-D-Glc*p*A-(1 → 3	4.6/94.9	3.3/72.3	3.6/84.0	3.5/70.9	3.6/76.4	−/175.6

3.3. The expression of metastasis-associated molecular markers

Overexpression and activation of focal adhesion kinase (FAK) contribute to cancer metastasis [38]. To assess the activity of FAK and downstream signaling pathways in A549 cells upon LAO, FAK/PI3K/Akt/mTOR signaling-associated proteins, including FAK, PI3K, AKT, P-AKT, TSC2 and mTOR were investigated by Western blotting. Fig. 4D and E show that up-regulated protein levels of TSC2 were only observed at the concentration of 3.80 mg/mL. FAK, PI3K, P-AKT and mTOR were significantly down-regulated at the different concentrations. It was worth noting that AKT showed no obvious change.

3.4. SPR solution competition study between LAO and growth factors

A very strong inhibitory activity (>80%) was observed for FGF1 at the concentration of 0.5 mg/mL (Fig. 5A and B). The half maximal inhibitory

Table 2
Proposed compositions of the ions of LAO.

m/z	Composition	m/z	Composition
338.049	$[GlcA_4\text{-}CO_2\text{-}2H]^{2-}$	689.104	$[GlcA_7OX_3\text{-}2H]^{2-}$
359.055	$[GlcA_3OX\text{-}2H]^{2-}$	703.124	$[GlcA_8\text{-}H_2O\text{-}2H]^{2-}$
425.058	$[GlcA_4OX_3\text{-}2H]^{2-}$	711.120	$[GlcA_7OX\text{-}2H]^{2-}$
447.071	$[GlcA_4OX\text{-}2H]^{2-}$	769.124	$[GlcA_9\text{-}CO_2\text{-}H_2O\text{-}2H]^{2-}$
513.074	$[GlcA_5OX_3\text{-}2H]^{2-}$	791.142	$[GlcA_9\text{-}H_2O\text{-}2H]^{2-}$
535.087	$[GlcA_5OX\text{-}2H]^{2-}$	857.141	$[GlcA_{10}\text{-}CO_2\text{-}H_2O\text{-}2H]^{2-}$
543.058	$[GlcA_5OX_1\text{-}2H]^{2-}$	879.157	$[GlcA_{10}\text{-}H_2O\text{-}2H]^{2-}$
586.087	$[GlcA_6Glc\text{-}CO_2\text{-}H_2O\text{-}2H]^{2-}$	895.150	$[GlcA_9OX_1\text{-}2H]^{2-}$
594.101	$[GlcA_5GlcOX_3\text{-}2H]^{2-}$	967.173	$[GlcA_{11}\text{-}H_2O\text{-}2H]^{2-}$
601.091	$[GlcA_6OX_3\text{-}2H]^{2-}$	975.170	$[GlcA_{10}OX\text{-}2H]^{2-}$
623.103	$[GlcA_6OX\text{-}2H]^{2-}$	1142.194	$[GlcA_{12}OX\text{-}H_2O\text{-}2H]^{2-}$
631.099	$[GlcA_6OX_1\text{-}2H]^{2-}$		

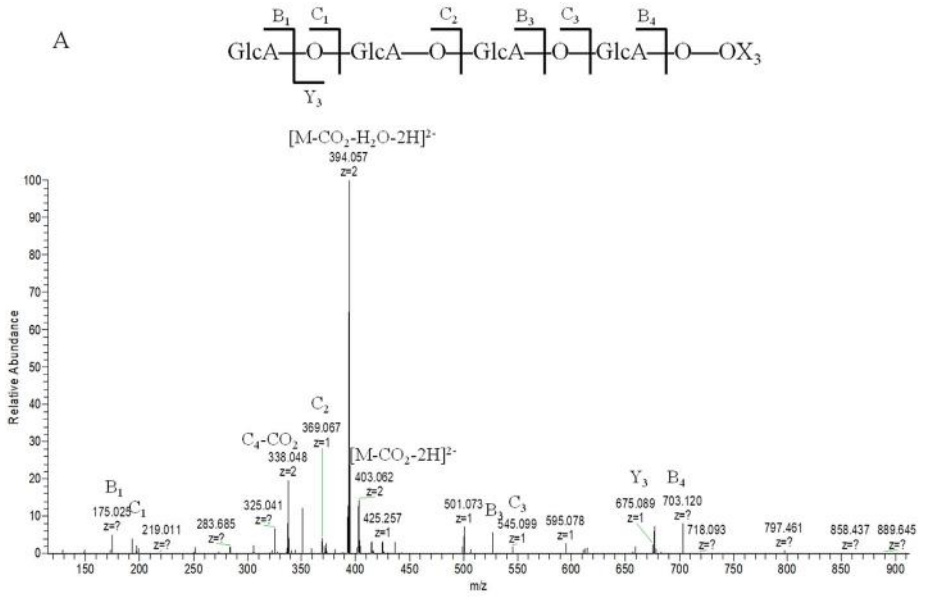
A
GlcA
GlcA
GlcA
GlcA
OX3
[M-CO2-H2O-2H]2-
394.057
z=2
Relative Abundance
m/z

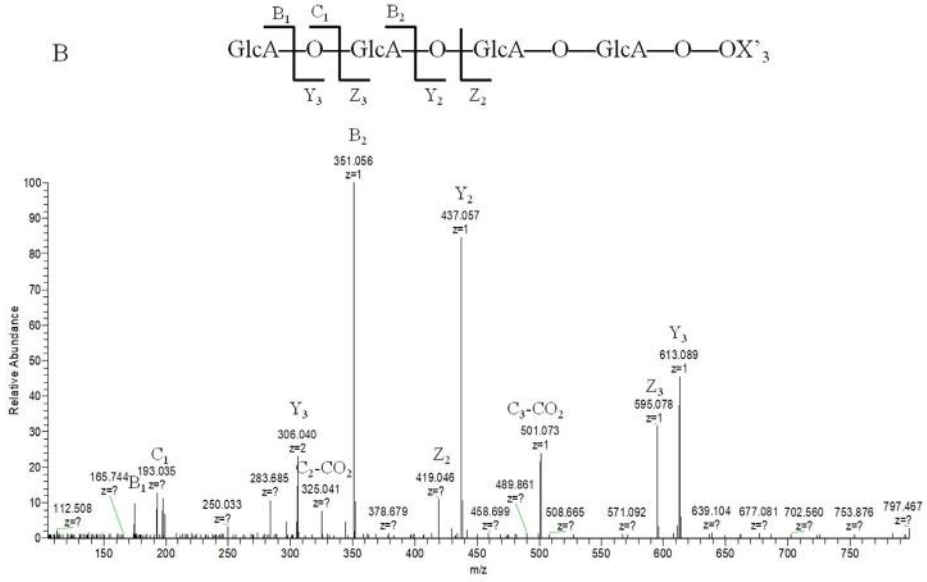
B
GlcA
GlcA
GlcA
GlcA
OX'3
Relative Abundance
m/z

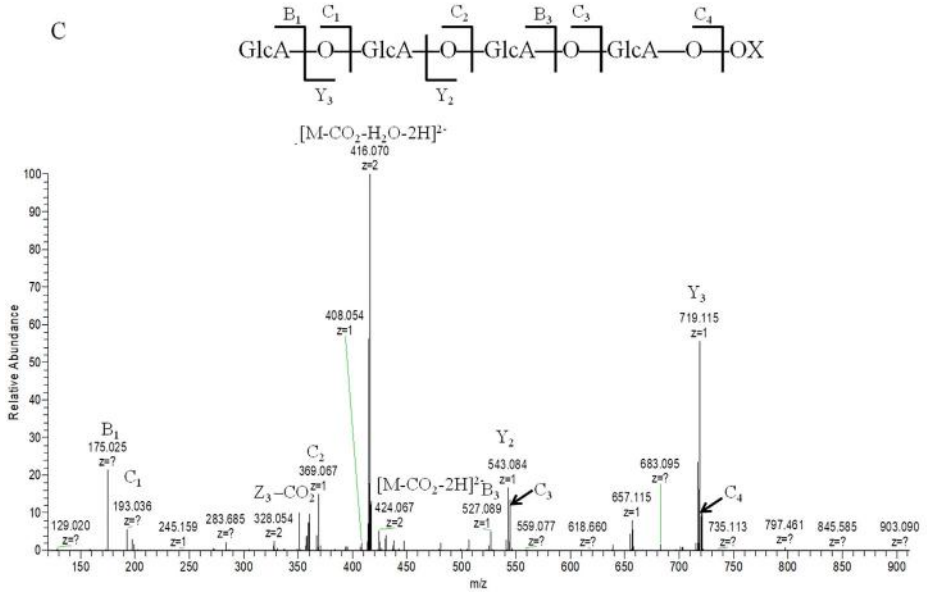
C
GlcA
GlcA
GlcA
GlcA
OX
[M-CO2-H2O-2H]2-
416.070
z=2
Relative Abundance
m/z

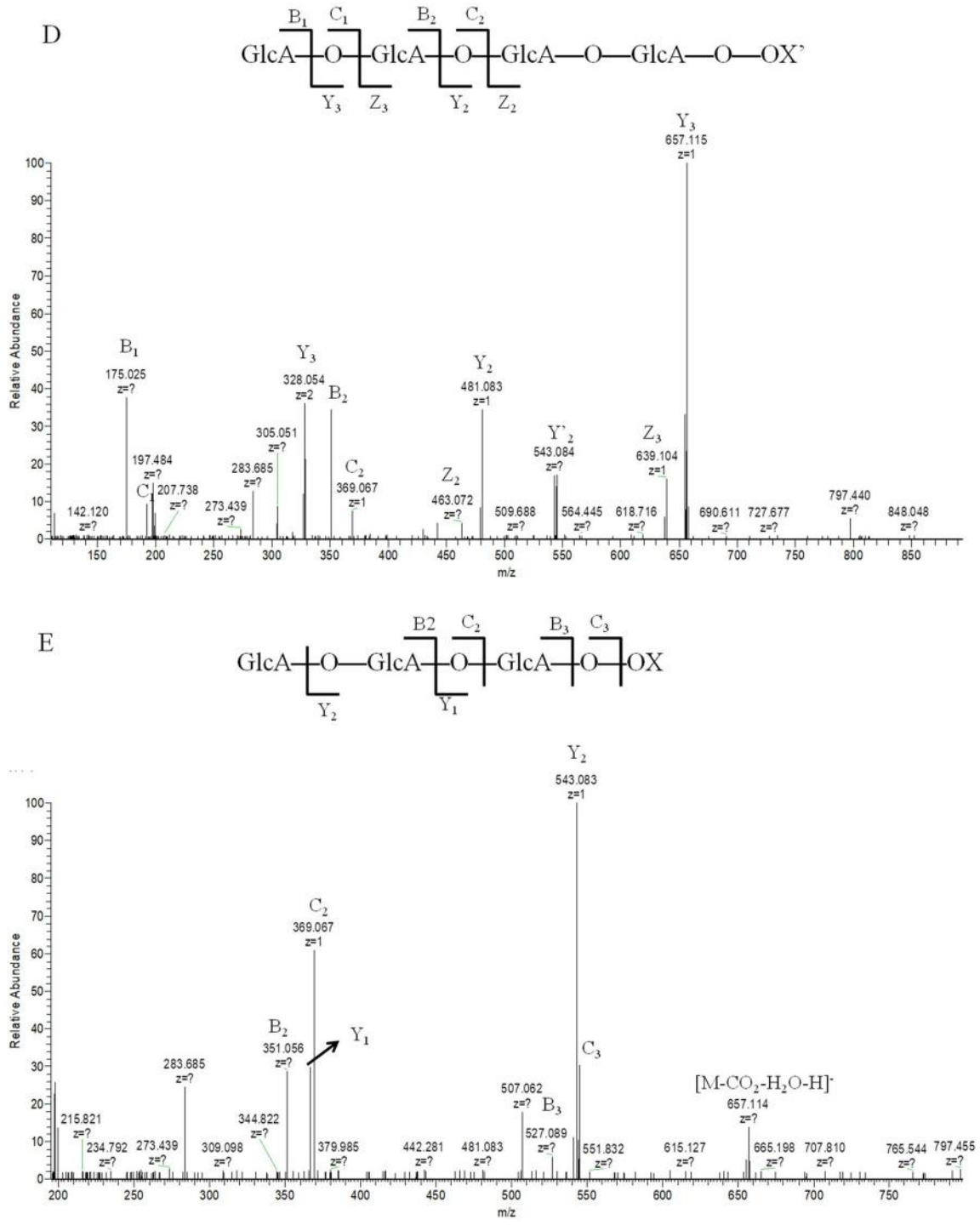

Fig. 3. Negative-ion mode ESI-CID- MS^n spectra of the ions at *m/z* 425.058 $[GlcA_4OX_3\text{-}2H]^{2-}$ (A), 394.057 $[GlcA_4OX_3\text{-}CO_2\text{-}H_2O\text{-}2H]^{2-}$ (B), 447.071 $[GlcA_4OX\text{-}2H]^{2-}$ (C), 416.070 $[GlcA_4OX\text{-}CO_2\text{-}H_2O\text{-}2H]^{2-}$ (D) and 719.115 $[GlcA_4OX\text{-}GlcA\text{-}H]^{1-}$ (E).

concentration (IC_{50}) was 0.07 mg/mL. FGF2 showed no concentration dependent inhibition and the inhibitory activity was fluctuated between 15% and 28% (Fig. 5C and D).

4. Discussion

Purified laminarin (LA) is obtained from *Sargassum thunbergii*. TEMPO-mediated reaction was carried out to oxidize the C6 position of Glc*p* into Glc*p*A, resulting in a new glucoglucuronan (LAO). The reducing end of LA was also oxidized, however, some byproducts at the reducing end were treated with 1 M trifluoroacetic acid.

Lung cancer, as the leading cause of cancer mortality, attracts much attention in research laboratories [39]. In the ten leading cancer types, it is estimated new lung and bronchus cancer cases will account for 23% in men and 22% in women in the United States in 2020. Most lung cancers are categorized as small cell lung cancer (SCLC) and non-SCLC, accounting for approximately 80% of all lung cancer cases [40]. Therefore, the inhibition by LAO on A549 cell proliferation has been determined *in vitro*. LAO markedly inhibited the growth of A549 cells in a dose-dependent manner.

Many studies have shown that FAK, as a central mediator of integrin-related signaling pathway, plays a critical role in regulating cancer cell

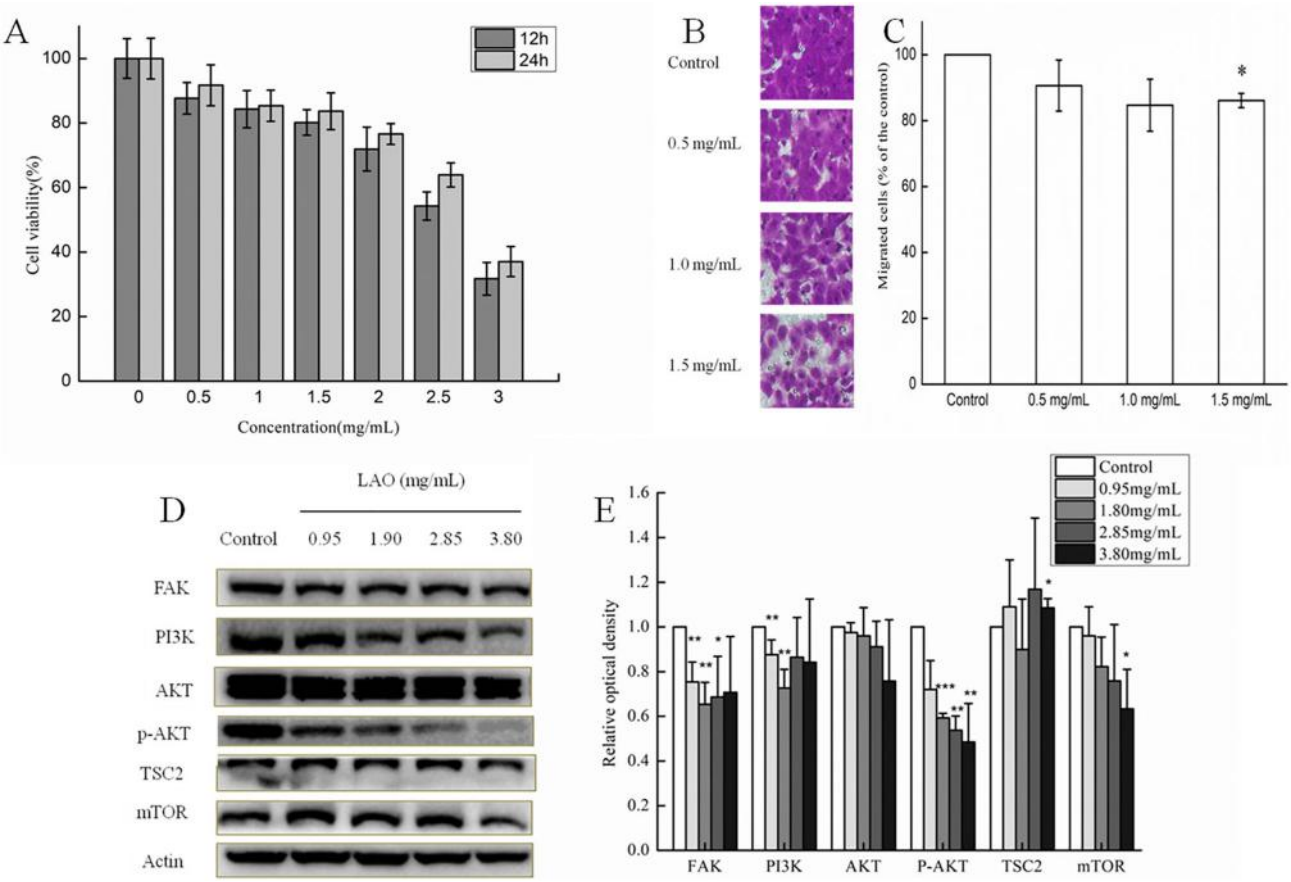

Fig. 4. (A) Concentration- and time-dependent cytotoxic effects of LAO on A549 cells. Cells were cultured in 96-well plate and treated with different doses of LAO (0–3.0 mg/mL) for 12 and 24 h. (B) Representative images of the cell migration induced by LAO in transwell migration assay. (C) Quantitative evaluation of the cell migration induced by LAO in transwell migration assay. Values shown are means ± SD ($n = 3$). $^{*}P < 0.05$ *vs.* control group. (D) Effects of LAO on protein expression of FAK, PI3K, AKT, P-AKT, TSC2 and mTOR in A549 cells. Representative images were acquired from three different experiments. (E) Quantitative analysis of the protein levels of FAK, PI3K, AKT, P-AKT, TSC2 and mTOR. Bars represent relative protein levels counted as D1/D0 (the value for control was set as 1.0), where D0 and D1 stand for the optical density of Actin (loading control) ladder and sample ladder, respectively. The optical density for each ladder was calculated by IMAGE J software. Data were obtained from three independent experiments. Values shown are means ± SD (n = 3). $^{*}P < 0.05$, $^{**}P < 0.01$ *vs.* control group.

migration, invasion, angiogenesis and epithelial-mesenchymal transition (EMT) [38,41]. FAK involves a key signaling protein-tyrosine kinase (PTK), which acts downstream of various growth factors and extracellular matrix (ECM) components. FAK promotes cell migration by the activation of multiple signaling pathways involving a kinase, or through the phosphorylation of other focal adhesion components [41,42]. FAK is also connected to the cytoskeleton through the ECM in focal adhesions [40,43]. Therefore, the adhesion of various cells will be influenced when FAK is weakened. Activation of mechanistic target of rapamycin (mTOR) signaling plays a crucial role in tumorigenesis of numerous malignancies [44]. mTOR, as one of important proteins in the downstream signaling pathways of FAK, forms two multi-protein complexes, mTORC1 and mTORC2, which are composed of discrete protein binding partners regulating cell growth, motility and metabolism [44]. mTORC1 is sensitive to nutrients and mTORC2 is regulated by PI3K and growth factor signaling. In this study, the expressions of FAK, PI3K, p-Akt, and mTOR in A549 cells decreased after LAO treatment, suggesting the involvement of FAK/PI3K/Akt/mTOR signaling pathways in the inhibitory effects of LAO in A549 cells. We also found only increased expression of TSC2, which would inhibit the expression of mTORC1.

The fibroblast growth factor (FGF) family are growth factors that play a vital role in cell development, transformation and tumorigenesis [45]. The most detailed investigations of the FGF interactions with heparan sulfate (HS) and heparin (HP) involve FGF1 and FGF2, providing the earliest *in vitro* experimental evidence for growth factors depending on an HS co-receptor [46]. The binding sites in FGF1 and FGF2 are similar in shape and composition, however, the interaction between FGF1/FGF2 and HS/HP are influenced by minor variations in proteins or HS/HP [46]. For example, FGF2 binds to the pentasaccharide (HexA-GlcNS-IdoA2S-GlcNS-IdoA), in which the IdoA2S residue is key [46–48]. However, 6-sulfo groups are required for interaction with FGF1 [46,49–51]. Therefore, it can be inferred that FGF1 and FGF2 recognizes specific patterns of sulfation as distinct from binding affinities and is mainly dependent on sulfate density [46]. Unlike HS/HP, LAO has no sulfate group. It is hard to explain why LAO interacts strongly with FGF1 but not with FGF2, because FGF1 requires a HS/HP with 6-sulfo groups and FGF2 requires HP/HS with IdoA2S residues. Therefore, we suggest that the glucuronic acid residues of LAO interact with FGF1 and FGF2, in place of the sulfate groups. Further experiments are planned to better understand this phenomenon.

5. Conclusion

A new glucoglucuronan, LAO, was prepared from LA by TEMPO-mediated oxidation. It was shown that LAO mainly had a major backbone of (1 → 3)-linked β-D-Glc*p*A interspersed with (1 → 3, 1 → 6)-linked β-D-Glc*p*, which was terminated with β-D-Glc*p*A. In addition, LAO can inhibit the proliferation through FAK/PI3K/AKT/mTOR pathway and strongly interact with FGF1.

Author contribution

Weihua Jin: Conceptualization, Methodology, Data curation, Formal analysis, Funding acquisition, Resources, Writing-Original draft

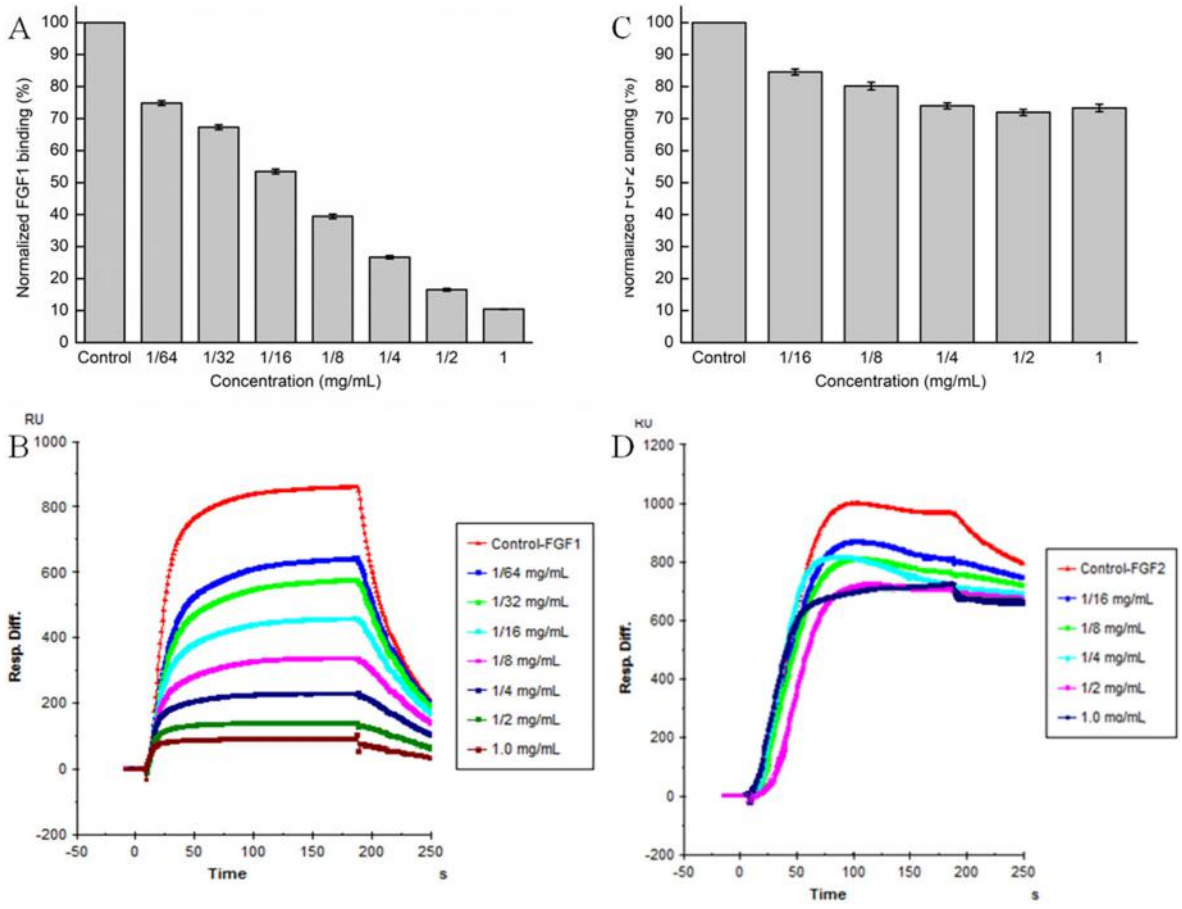

Fig. 5. Bar graphs and SPR sensorgrams of normalized different growth factors FGF1 (A and B) and FGF2 (C and D) binding preference to surface heparin by competing with different concentrations of LAO. Concentrations were 125 nM and 100 nM for FGF1 and FGF2, respectively. Data are presented as means ± SD of three independent experiments ($n = 3$).

preparation, Project administration; **Xinyue He:** Conceptualization, Methodology; **Wanli Wu:** Conceptualization, Methodology; **Yizhong Bao**: Conceptualization, Methodology; **Sanying Wang**: Conceptualization, Methodology; **Min Cai**: Conceptualization, Methodology; **Wenjing Zhang:** Methodology, Writing-Original draft preparation and Funding acquisition; **Chunyu Wang:** Writing-Reviewing and Editing; **Fuming Zhang:** Methodology, Writing Reviewing and Editing; **Robert J. Linhardt:** Writing-Reviewing and Editing, Funding acquisition; **Genxiang Mao:** Writing-Reviewing and Editing, Funding acquisition; **Weihong Zhong:** Writing-Reviewing, Editing and Supervision.

Acknowledgements

This study was supported by the Zhejiang Provincial Natural Science Foundation of China (No. LY19D060006); the National Natural Science Foundation of China (Nos. 41906095, 41506165 and 81771520); China Scholarship Council (W.J.) and the National Institutes of Health (DK111958 and CA231074).

Declaration of competing interest

The authors declare no conflicts of interest.

Appendix A. Supplementary data

Supplementary data to this article can be found online at https://doi.org/10.1016/j.ijbiomac.2020.07.069.

References

[1] W. Jin, G. Liu, W. Zhong, C. Sun, Q. Zhang, Polysaccharides from *Sargassum thunbergii*: monthly variations and anti-complement and anti-tumour activities, Int. J. Biol. Macromol. 105 (2017) 1526–1531.
[2] M. Zargarzadeh, A.J.R. Amaral, C.A. Custodio, J.F. Mano, Biomedical applications of laminarin, Carbohydr. Polym. 232 (2020), 115774. .
[3] K.K.A. Sanjeewa, J.S. Lee, W.S. Kim, Y.J. Jeon, The potential of brown-algae polysaccharides for the development of anticancer agents: an update on anticancer effects reported for fucoidan and laminaran, Carbohydr. Polym. 177 (2017) 451–459.
[4] R.V. Usoltseva, N.M. Shevchenko, O.S. Malyarenko, I.A. Ishina, S.I. Ivannikova, S.P. Ermakova, Structure and anticancer activity of native and modified polysaccharides from brown alga *Dictyota dichotoma*, Carbohydr. Polym. 180 (2018) 21–28.
[5] K. Song, L. Xu, W. Zhang, Y. Cai, B. Jang, J. Oh, J.O. Jin, Laminarin promotes anti-cancer immunity by the maturation of dendritic cells, Oncotarget 8 (2017) 38554–38567.
[6] A.J. Smith, B. Graves, R. Child, P.J. Rice, Z. Ma, D.W. Lowman, H.E. Ensley, K.T. Ryter, J.T. Evans, D.L. Williams, Immunoregulatory activity of the natural product laminarin varies widely as a result of its physical properties, J. Immunol. 200 (2018) 788–799.
[7] Y.L. Shih, S.C. Hsueh, Y.L. Chen, J.S. Chou, H.Y. Chung, K.L. Liu, H.W. Jair, Y.Y. Chuang, H.F. Lu, J.Y. Liu, J.G. Chung, Laminarin promotes immune responses and reduces lactate dehydrogenase but increases glutamic pyruvic transaminase in normal mice in vivo, In Vivo 32 (2018) 523–529.
[8] R.V. Menshova, S.P. Ermakova, S.D. Anastyuk, V.V. Isakov, Y.V. Dubrovskaya, M.I. Kusaykin, B.H. Um, T.N. Zvyagintseva, Structure, enzymatic transformation and anticancer activity of branched high molecular weight laminaran from brown alga *Eisenia bicyclis*, Carbohydr. Polym. 99 (2014) 101–109.
[9] J. Li, C. Cai, C. Yang, J. Li, T. Sun, G. Yu, Recent advances in pharmaceutical potential of brown algal polysaccharides and their derivatives, Curr. Pharm. Des. 25 (2019) 1290–1311.
[10] H. Duan, M. Donovan, A. Foucher, X. Schultze, S. Lecommandoux, Multivalent and multifunctional polysaccharide-based particles for controlled receptor recognition, Sci. Rep. 8 (2018), 14730. .
[11] O.S. Malyarenko, R.V. Usoltseva, T.N. Zvyagintseva, S.P. Ermakova, Laminaran from brown alga *Dictyota dichotoma* and its sulfated derivative as radioprotectors and radiosensitizers in melanoma therapy, Carbohydr. Polym. 206 (2019) 539–547.

[12] W. Jin, W. Zhang, H. Liang, Q. Zhang, The structure-activity relationship between marine algae polysaccharides and anti-complement activity, Mar Drugs 14 (2015) 3.
[13] F. Paris, S. Trouvelot, M. Jubien, G. Lecollinet, J.M. Joubert, A. Chiltz, M.C. Heloir, J. Negrel, M. Adrian, L. Legentil, X. Daire, V. Ferrieres, Hydrophobized laminarans as new biocompatible anti-oomycete compounds for grapevine protection, Carbohydr. Polym. 225 (2019), 115224. .
[14] D. Cui, J. Ma, T. Liang, L. Sun, L. Meng, T. Liang, Q. Li, Selenium nanoparticles fabricated in laminarin polysaccharides solutions exert their cytotoxicities in HepG2 cells by inhibiting autophagy and promoting apoptosis, Int. J. Biol. Macromol. 137 (2019) 829–835.
[15] C.R. Martins, C.A. Custodio, J.F. Mano, Multifunctional laminarin microparticles for cell adhesion and expansion, Carbohydr. Polym. 202 (2018) 91–98.
[16] X. Song, M.A. Hubbe, TEMPO-mediated oxidation of oat beta-D-glucan and its influences on paper properties, Carbohydr. Polym. 99 (2014) 617–623.
[17] P. Ma, S. Fu, H. Zhai, K. Law, C. Daneault, Influence of TEMPO-mediated oxidation on the lignin of thermomechanical pulp, Bioresour. Technol. 118 (2012) 607–610.
[18] R. Tanaka, T. Saito, A. Isogai, Cellulose nanofibrils prepared from softwood cellulose by TEMPO/NaClO/NaClO(2) systems in water at pH 4.8 or 6.8, Int. J. Biol. Macromol. 51 (2012) 228–234.
[19] Y. Zhou, T. Saito, L. Bergstrom, A. Isogai, Acid-free preparation of cellulose nanocrystals by TEMPO oxidation and subsequent cavitation, Biomacromolecules 19 (2018) 633–639.
[20] S.S. Lal, S.T. Mhaske, AgBr and AgCl nanoparticle doped TEMPO-oxidized microfiber cellulose as a starting material for antimicrobial filter, Carbohydr. Polym. 191 (2018) 266–279.
[21] R. Tang, J. Hao, R. Zong, F. Wu, Y. Zeng, Z. Zhang, Oxidation pattern of curdlan with TEMPO-mediated system, Carbohydr. Polym. 186 (2018) 9–16.
[22] P.S. Chang, K.O. Park, H.K. Shin, D.S. Suh, K.O. Kim, Physicochemical properties of partially oxidized corn starch from bromide-free TEMPO-mediated reaction, J. Food Sci. 73 (2008) C173–C178.
[23] Y. Fan, T. Saito, A. Isogai, Chitin nanocrystals prepared by TEMPO-mediated oxidation of alpha-chitin, Biomacromolecules 9 (2008) 192–198.
[24] B. Ding, Y. Ye, J. Cheng, K. Wang, J. Luo, B. Jiang, TEMPO-mediated selective oxidation of substituted polysaccharides–an efficient approach for the determination of the degree of substitution at C-6, Carbohydr. Res. 343 (2008) 3112–3116.
[25] L. Guentas, P. Pheulpin, A. Heyraud, C. Gey, B. Courtois, J. Courtois, Production of a glucoglucuronan by a rhizobia strain infecting alfalfa. Structure of the repeating unit, Int. J. Biol. Macromol. 27 (2000) 269–277.
[26] E. Petit, D. Papy-Garcia, G. Muller, B. Courtois, J.P. Caruelle, J. Courtois, Controlled sulfatation of natural anionic bacterial polysaccharides can yield agents with specific regenerating activity in vivo, Biomacromolecules 5 (2004) 445–452.
[27] E. Redouan, P. Emmanuel, M. Philippe, C. Bernard, C. Josiane, D. Cedric, Synthesis of new glycosaminoglycans-like families by regioselective oxidation followed by sulphation of glucoglucuronan from *Rhizobium sp.* T1, Carbohydr. Polym. 89 (2012) 1261–1267.
[28] Y.-T. Kim, E.-H. Kim, C. Cheong, D.L. Williams, C.-W. Kim, S.-T. Lim, Structural characterization of β-d-(1→3, 1→6)-linked glucans using NMR spectroscopy, Carbohydr. Res. 328 (2000) 331–341.
[29] W. Jin, B. Liu, S. Li, J. Chen, H. Tang, D. Jiang, Q. Zhang, W. Zhong, The structural features of the sulfated heteropolysaccharide (ST-1) from *Sargassum thunbergii* and its neuroprotective activities, Int. J. Biol. Macromol. 108 (2018) 307–313.
[30] J. Hao, J. Lu, N. Xu, R.J. Linhardt, Z. Zhang, Specific oxidation pattern of soluble starch with TEMPO-NaBr-NaClO system, Carbohydr. Polym. 146 (2016) 238–244.
[31] J. Zhang, Q. Zhang, J. Wang, X. Shi, Z. Zhang, Analysis of the monosaccharide composition of fucoidan by precolumn derivation HPLC, Chin. J. Oceanol. Limnol. 27 (2009) 1–5.
[32] G. Liu, S. Kuang, S. Wu, W. Jin, C. Sun, A novel polysaccharide from Sargassum integerrimum induces apoptosis in A549 cells and prevents angiogensis in vitro and in vivo, Sci. Rep. 6 (2016) 26722.
[33] G. Mao, H. Li, X. Ding, X. Meng, G. Wang, S.X. Leng, Suppressive effects of sirtinol on human cytomegalovirus (hCMV) infection and hCMV-induced activation of molecular mechanisms of senescence and production of reactive oxygen species, Mech. Ageing Dev. 158 (2016) 62–69.
[34] F. Zhang, L. Zheng, S. Cheng, Y. Peng, L. Fu, X. Zhang, R.J. Linhardt, Comparison of the interactions of different growth factors and glycosaminoglycans, Molecules 24 (2019).
[35] W. Jin, W. Zhang, J. Wang, S. Ren, N. Song, D. Duan, Q. Zhang, Characterization of laminaran and a highly sulfated polysaccharide from *Sargassum fusiforme*, Carbohydr. Res. 385 (2014) 58–64.
[36] R. Zhang, X. Zhang, Y. Tang, J. Mao, Composition, isolation, purification and biological activities of *Sargassum fusiforme* polysaccharides: a review, Carbohydr. Polym. 228 (2020), 115381. .
[37] S. Komulainen, C. Verlackt, J. Pursiainen, M. Lajunen, Oxidation and degradation of native wheat starch by acidic bromate in water at room temperature, Carbohydr. Polym. 93 (2013) 73–80.
[38] T.Y. Yang, M.L. Wu, C.I. Chang, C.I. Liu, T.C. Cheng, Y.J. Wu, Bornyl cis-4-hydroxycinnamate suppresses cell metastasis of melanoma through FAK/PI3K/Akt/mTOR and MAPK signaling pathways and inhibition of the epithelial-to-mesenchymal transition, Int. J. Mol. Sci. 19 (2018).
[39] R.L. Siegel, K.D. Miller, A. Jemal, Cancer statistics, 2020, CA Cancer J. Clin. 70 (2020) 7–30.
[40] H. Zhao, G. Chen, L. Ye, H. Yu, S. Li, W.G. Jiang, DOK7V1 influences the malignant phenotype of lung cancer cells through PI3K/AKT/mTOR and FAK/paxillin signaling pathways, Int. J. Oncol. 54 (2019) 381–389.
[41] Y.L. Hu, S. Lu, K.W. Szeto, J. Sun, Y. Wang, J.C. Lasheras, S. Chien, FAK and paxillin dynamics at focal adhesions in the protrusions of migrating cells, Sci. Rep. 4 (2014) 6024.
[42] D.J. Sieg, C.R. Hauck, D. Ilic, C.K. Klingbeil, E. Schaefer, C.H. Damsky, D.D. Schlaepfer, FAK integrates growth-factor and integrin signals to promote cell migration, Nat. Cell Biol. 2 (2000) 249–256.
[43] S.K. Mitra, D.A. Hanson, D.D. Schlaepfer, Focal adhesion kinase: in command and control of cell motility, Nat Rev Mol Cell Biol 6 (2005) 56–68.
[44] M. Jhanwar-Uniyal, J.V. Wainwright, A.L. Mohan, M.E. Tobias, R. Murali, C.D. Gandhi, M.H. Schmidt, Diverse signaling mechanisms of mTOR complexes: mTORC1 and mTORC2 in forming a formidable relationship, Adv Biol Regul 72 (2019) 51–62.
[45] M. Cross, T.M. Dexter, Growth factors in development, transformation, and tumorigenesis, Cell 64 (1991) 271–280.
[46] J. Gallagher, Fell-Muir lecture: heparan sulphate and the art of cell regulation: a polymer chain conducts the protein orchestra, Int. J. Exp. Pathol. 96 (2015) 203–231.
[47] S. Faham, R.E. Hileman, J.R. Fromm, R.J. Linhardt, D.C. Rees, Heparin structure and interactions with basic fibroblast growth factor, Science 271 (1996) 1116–1120.
[48] M. Maccarana, B. Casu, U. Lindahl, Minimal sequence in heparin/heparan sulfate required for binding of basic fibroblast growth factor, J. Biol. Chem. 268 (1993) 23898–23905.
[49] J. Kreuger, M. Salmivirta, L. Sturiale, G. Gimenez-Gallego, U. Lindahl, Sequence analysis of heparan sulfate epitopes with graded affinities for fibroblast growth factors 1 and 2, J. Biol. Chem. 276 (2001) 30744–30752.
[50] M. Guerrini, T. Agulles, A. Bisio, M. Hricovini, L. Lay, A. Naggi, L. Poletti, L. Sturiale, G. Torri, B. Casu, Minimal heparin/heparan sulfate sequences for binding to fibroblast growth factor-1, Biochem. Biophys. Res. Commun. 292 (2002) 222–230.
[51] S. Ashikari-Hada, H. Habuchi, Y. Kariya, N. Itoh, A.H. Reddi, K. Kimata, Characterization of growth factor-binding structures in heparin/heparan sulfate using an octasaccharide library, J. Biol. Chem. 279 (2004) 12346–12354.